The Journal of CPRI,
Vol. 11, No. 2, June 2015 pp. 323-332

Design of high temperature induction motor for application in sodium cooled fast reactor control system

Nashine B K*, Rajendra Prasad*, Vijay Sharma* and B P C Rao*

Prototype Fast Breeder Reactor (PFBR) employs induction motors of various power ratings in high temperature ambient and sometimes corrosive atmosphere. Safe operation of the reactor depends on robustness and reliability of induction motors in its critical components. Safety related systems such as shutdown and online inspection systems, utilize induction motors as actuators in their mechanisms. Since external cooling is not permitted in control and inspection motors, special design of motors is required to withstand high temperatures. This paper deals with design, analysis, fabrication and testing of a compact 50 W, three phase induction motor, suitable for operating up to 250 °C ambient with winding temperature withstand capability up to 550°C. The designed motor was analyzed with two dimensional Finite Element Model (FEM) code FEMM to study the torque slip characteristics and magnetic flux density patterns in stator and rotor.

Keywords: *Induction motor, high temperature, FEM Analysis, MI cable*

1.0 INTRODUCTION

Fast breeder reactors constitute the second stage of India's three stage nuclear program for effective utilization of the country's limited reserves of natural uranium and exploitation of its large reserves of thorium. A 40 MWt/13 MWe loop type Fast Breeder Test Reactor (FBTR) [1] was commissioned in 1985 at Kalpakkam and as next step in Fast breeder technology, PFBR is being constructed at the same site [2]. Liquid sodium is used as coolant in both loop type FBTR and pool type PFBR. Prototype Fast Breeder Reactor (PFBR) is a 500 MWe, sodium cooled, pool type, mixed oxide (MOX) fueled reactor. PFBR utilizes various electrical and instrumentation equipments for it's safe and reliable operation [3-6]. Electric motors of different ratings are used as actuators in shut down mechanisms and instrumentation systems. Electric motors are also required for device used for in-service inspection of the reactor under high temperature and in fuel cycle facility, where acidic and radiation environment is present.

Three phase Induction motor are used in many critical components of PFBR due to their rugged construction, less maintenance and fairly constant speed. High temperatures and corrosive environment require special design features compared to conventional induction motors. Computational methods such as finite element modeling (FEM) are used extensively for design, optimization and parametric analysis of three phase induction motors. FEM in induction motors involves magnetic field analysis in which the magnetic circuit geometry, spatial distribution of stator windings and rotor bars and nonlinear behavior of ferromagnetic materials is taken into account [7]. FEM was used to study magnetic flux, flux density distribution and saturation in stator and rotor of induction motors [8]. FEM was

*Indira Gandhi Centre for Atomic Research, Kalpakkam - 603 102, Tamil Nadu, India. Phone: +91 44 27495217, E-mail: bknash@igcar.gov.in

also used to study and monitor the steady state [9] and dynamic performance of the motor [10].

The study of heating problems of induction motors and the prediction of temperature rise of magnetic core, teeth, insulation, conductors, etc. was done by Sarkar and Naskar [11]. The authors presented a two-dimensional transient heat flow in the stator of a squirrel cage induction motor. A temperature–time method was employed to evaluate the distribution of loss in various parts of the machine. These loss distributions were used as an input for finite element analysis to predict more accurate temperature distributions. FEM was also used by Ying Xie and Yunyang Wang to study the effect of rotor bar fault on motor performance [12]. The losses in motor were determined from a complex finite element analysis of the magnetic field and the three dimensional thermal models of the induction motor operating at the healthy state, one broken bar fault and two adjacent broken bars fault state were analyzed.

In this work, design, fabrication and testing of a compact three phase 50 W, 110 V, 3600 rpm squirrel cage induction motor with Mineral Insulated (MI) cable winding is discussed. The work was carried out in two stages, in first stage, one compact induction motor with class H insulation winding was developed. After testing the performance of the motor, stator windings of the motor were replaced with MI cable winding to make it suitable for operation in acidic and high temperature environment. The designed motor for high temperature applications was analyzed in FEM code FEMM to study the effects of reduction in space factor with MI cable as stator windings on different electrical parameters. The paper discusses design, fabrication, testing and analysis of MI cable wound induction motor capable of withstanding high temperatures.

2.0 INDUCTION MOTOR WITH CLASS H INSULATION

2.1 Induction Motor Design

One 50 Watt, 3 phase, 110 Volt, 3600 rpm, squirrel cage induction motor was designed as per specifications given in Table 1. The overall dimensions of the motor were fixed as per process requirements. CRNGO laminations of 0.35 mm thickness were used to form the stator core and stator teeth of desired dimensions to avoid magnetic saturation of stator of the motor. Insulation of stator winding was Class H type. Stator frame, which encloses stator core and windings and transmit the motor load to machine supports was made of Stainless Steel 316 (SS 316) to withstand high temperatures and corrosive environments. Twelve semi closed type stator slots were chosen to reduce the magnetizing current and tooth pulsation losses. Schematic of the stator cross section of the induction motor is shown in Figure 1. Salient equations used in stator design are given below.

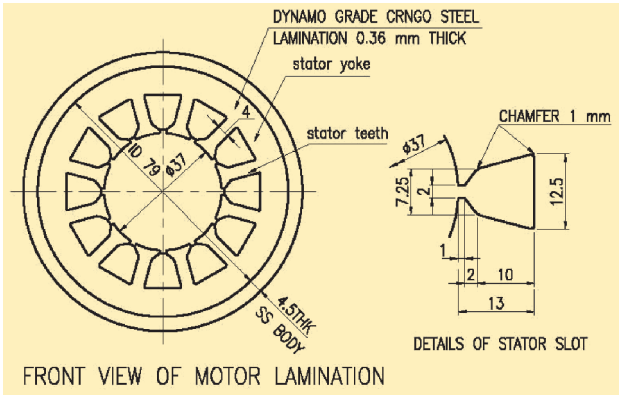

FIG. 1 CROSS SECTIONAL VIEW OF STATOR

TABLE 1

Sl. No.	SPECIFICATIONS OF THE MOTOR	
1	Power	50 Watts
2	Voltage (line to line)	110 Volts
3	Rated Phase current	0.9 A
4	Phase	3 phase
5	Frequency	65 Hz
6	Motor Syn Speed	3900 rpm
7	Insulation type	Class H
8	OD of motor	88 mm
9	Length of motor	164 mm (body)
10	Length of rotor shaft	262.2 mm
11	Outer body of motor	SS 316
12	Laminations	0.35 mm (CRNGO)
13	Bare copper conductor (Dia)	0.63 mm
14	Enamelled copper wire (Dia)	0.85 mm

$$Q = KVA\ input = \frac{Motor\ power\ output}{\eta \times \cos(\emptyset)} \quad ....(1)$$

$$D^2L = \frac{Q}{C_0 n_s} \quad ....(2)$$

$$C_0 = 11 \times K_w \times B_{av} \times ac \times 10^{-3} \quad ....(3)$$

$$Pole\ Pitch\ (\tau) = \frac{\pi D}{P} \quad ....(4)$$

$$Flux\ per\ pole(\emptyset_m) = B_{av} \times \tau \times L \quad ....(5)$$

$$Flux\ density\ at\ stator\ teeth = \frac{\emptyset_m}{1.7 \times \frac{Ss}{p} \times L_i} \quad ....(6)$$

$$Turns\ per\ phase\ (T_{ph}) = \frac{E_s}{4.44 \times f \times \emptyset_m \times K_w} \quad ....(7)$$

$$Stator\ current\ per\ phase\ Is\ \frac{Q(input\ KVA)}{\sqrt{3} \times V_L} \quad ....(8)$$

$$Current\ density\ in\ stator = \frac{I_s}{a_s} \quad ....(9)$$

where

C_0	Output coefficient
D	Armature diameter or stator bore
L	Stator core length
η	Efficiency
cos (ø)	Power factor
P	Number of poles
K_w	Winding factor
B_{av}	Specific magnetic loading
τ	Pole pitch
ac	Specific electric loading
n_s	Synchronous speed (r.m.s)
f	Frequency
Ss	Number of stator slots
L_i	Net iron length
V_L	Line voltage
I_s	Stator line current

CRNGO laminations of 0.35 mm thickness, die cast Aluminium rotor bar and end rings were used in rotor of the motor. Rotor with seventeen semi closed rectangular slots was chosen for better overload capacity and high starting torque. Schematics of rotor cross section are shown in Figure 2 and Figure 3. Rotor bars shape chosen helps in higher starting torque and lower operating losses. Pictorial view of the developed low power induction motor is shown in Figure 4. Equations used for rotor design are given below.

$$l_g = 0.2 + 2\sqrt{DL} \quad ....(10)$$

$$D_r = D_{si} - 2 \times l_g \quad ....(11)$$

Where

l_g	Length of air gap
D_r	Diameter of rotor
D_{si}	Inner diameter of stator

$$Rotor\ slot\ pitch\ at\ air\ gap = \frac{\pi D}{Sr} \quad ....(12)$$

$$I_b = \frac{2 \times m_s \times K_{ws} \times T_{ph} \times I_s \times \cos(\emptyset)}{S_r} \quad ....(13)$$

$$a_b = \frac{I_b}{\delta_b} \quad ....(14)$$

$$B_{max}(Rotor\ teeth) = \frac{\emptyset_m}{\frac{S_r}{P} \times Rotor\ teeth \times L_i} \quad ....(15)$$

$$I_e = \frac{S_r I_b}{\pi P} \quad ....(16)$$

$$a_e = \frac{I_e}{\delta_b} \quad ....(17)$$

Where

I_b	Rotor bar current
a_b	Area of rotor bar
I_e	End ring current
a_e	Area of end ring
δ_b	Current density in rotor bar

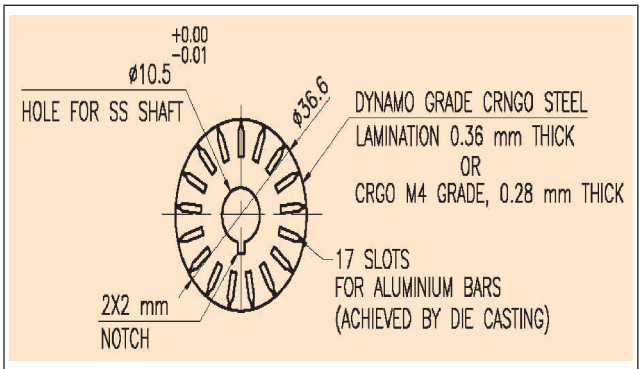

FIG. 2 CROSS SECTIONAL VIEW ROTOR

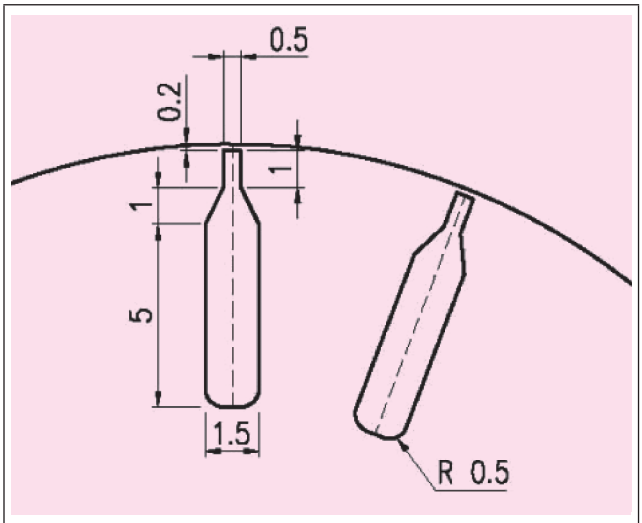

FIG. 3 CROSS SECTIONAL VIEW ROTOR SLOT

FIG. 4 LOW POWER INDUCTION MOTOR

The developed motor was manufactured with design procedure given above and tested. The test set up for measuring different electrical parameters of the motor is shown in Figure5. Winding resistance of 1.5 Ω per phase was measured with 3 & 1/2 Digit Digital Multimeter. Insulation Resistance of induction motor was measured with 500 Volts DC Megger at room temperature. Current and power measurements at no load and locked rotor conditions of induction motor were conducted.

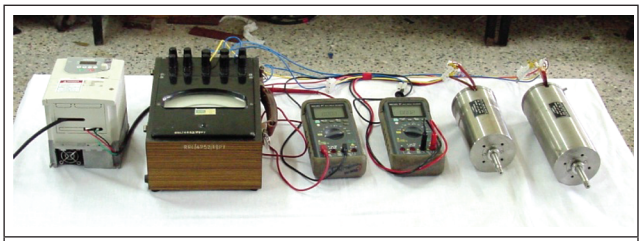

FIG. 5 TEST SET UP FOR INDUCTION MOTOR

3.0 DESIGN OF HIGH TEMPERATURE INDUCTION MOTOR WITH MINERAL INSULATED CABLE WINDING

After successful testing of the compact motor that met the space constraints and load requirements, the work on development of high temperature induction motor was taken up. The conventional winding of the already developed motor was replaced with mineral insulated cable winding. Stator windings of the motor was fabricated with Mineral Insulated (MI) cables of 1 mm outer diameter. MI cable consists of Stainless Steel (SS) sheath, MgO powder and copper conductor at the center of the cable. The MI cable do not undergo any major changes in the presence of radiation. The use of MI cables have been proved in different sensors used in liquid sodium cooled fast reactors for high temperature application up to 550°C [Bock and Suleiman, 1978; Prashant Sharma *et al.*, 2012]. Use of MI cable in electromagnets of the shut down systems submerged in sodium and operating at high temperatures is a classical example of suitability of MI cable under hostile environments [Rajan Babu *et al.,* 2010].

3.1 Properties and testing of MI cable

3.1.1 Properties of MI cable

MI cable consists of central copper conductor concentrically placed inside a SS tube. SS tube and central copper conductor are electrically insulated by a dense packing of highly pure Magnesium Oxide (MgO). The SS sheath of the required thickness on the cable is formed by drawing a single tube. Both ends of the cable are sealed using epoxy sealants. As per standards for MI cable minimum sheath thickness, minimum

cable core diameter and minimum insulation thickness is 10 %, 45 % and 12 % respectively of nominal outside diameter. MI cable was tested for conductor resistance, insulation resistance test at room and high temperatures, SS Sheath integrity and high voltage.

3.1.2 Current carrying capacity Teston MI Cable

In order to utilize the MI cable for high current density applications like induction motors, experiment was conducted to determine the current carrying capacity of the MI cable with outer diameter of 1.5 mm and conductor diameter of 0.8 mm. The schematic of the test set-up is shown in Figure 6 and the pictorial view of the test set-up is shown in Figure 7, Figure 8 and Figure 9. A thermocouple was used to monitor the temperature of the MI cable coil. Arheostat with ratings of 50 Ω and 10 Awas used in series with MI cable coil to vary the current in the coil.

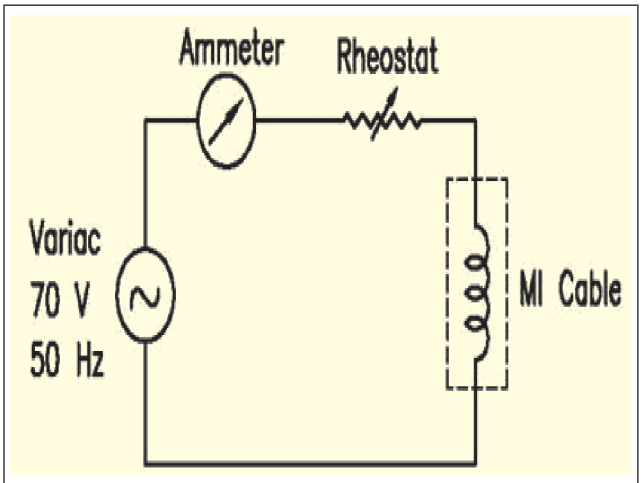

FIG. 6 SCHEMATIC OF TEST SET-UP FOR MI CABLE

During the testing, voltage up to 70 V was applied to the MI cable winding. The current in the winding was increased in steps by varying the resistance of rheostat and readings of thermocouple were recorded at regular intervals. Testing was done for 29 h with recording of temperatures at every one hour. Plot of current density verses current in MI cable and corresponding surface temperature is shown in Figure 10. It can be seen that MI cable is able to carry currents with current density up to 20 A/mm^2, which is much higher than conventional motor winding cable capability, which is in the range of 2 to 5 A/mm^2.

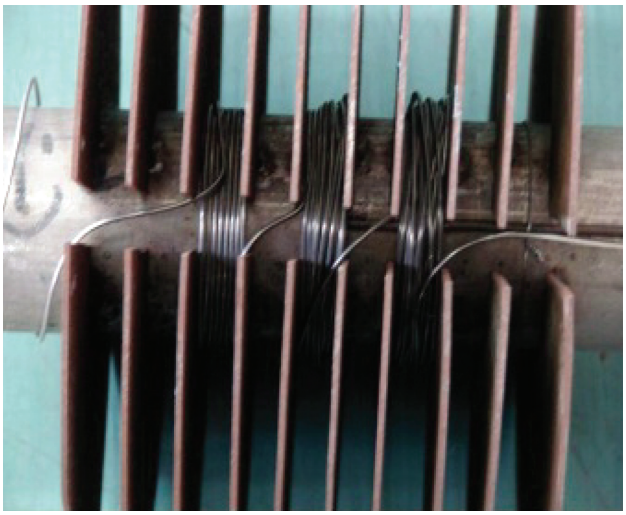

FIG. 7 MI CABLE IN WOUND CONDITION OVER A PIPE AND SLOT TYPE OF ARRANGEMENT

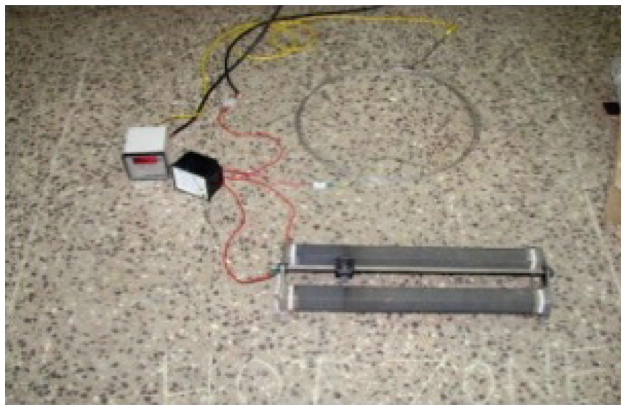

FIG. 8 TEST SET UP WITHOUT WOUND CONDITION

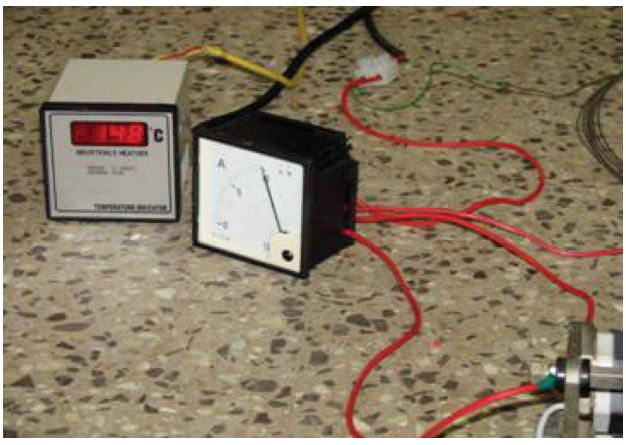

FIG. 9 THERMO-COUPLE READING AT 10 A

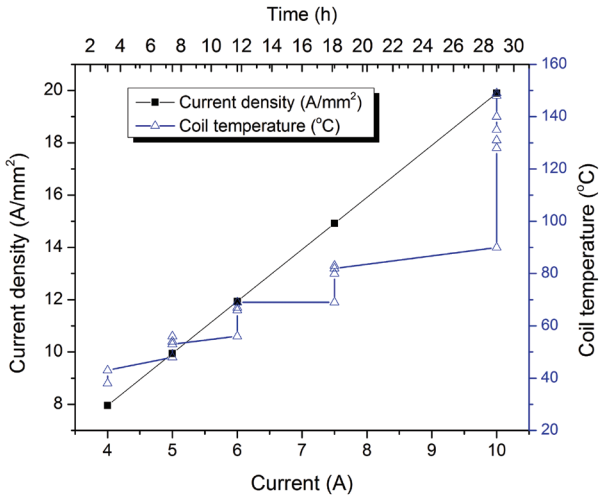

FIG. 10 CURRENT CARRYING CAPACITY OF MI CABLE

3.2 High Temperature induction motor with MI cable

Already designed stator frame and rotor was used for high temperature induction motor, except the stator winding, which is now made from MI cable. The stator outer diameter and length was maintained same due to process requirements.

3.2.1 Motor Design

Apart from stator windings, all other specifications of motor mentioned in section 2 were kept same as given in Table 1. Stator windings were formed with SS sheathed MI cable of 1 mm diameter with central copper conductor of 0.35 mm. Photographs of low power motor with MI cable winding are shown in Figure 11, Figure 12 and Figure 13.

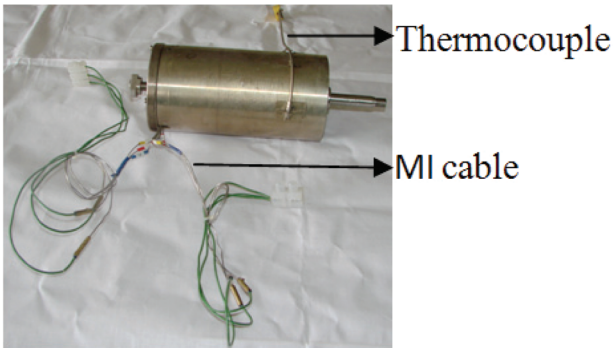

FIG. 11 LOW POWER INDUCTION MOTOR WITH MI CABLE

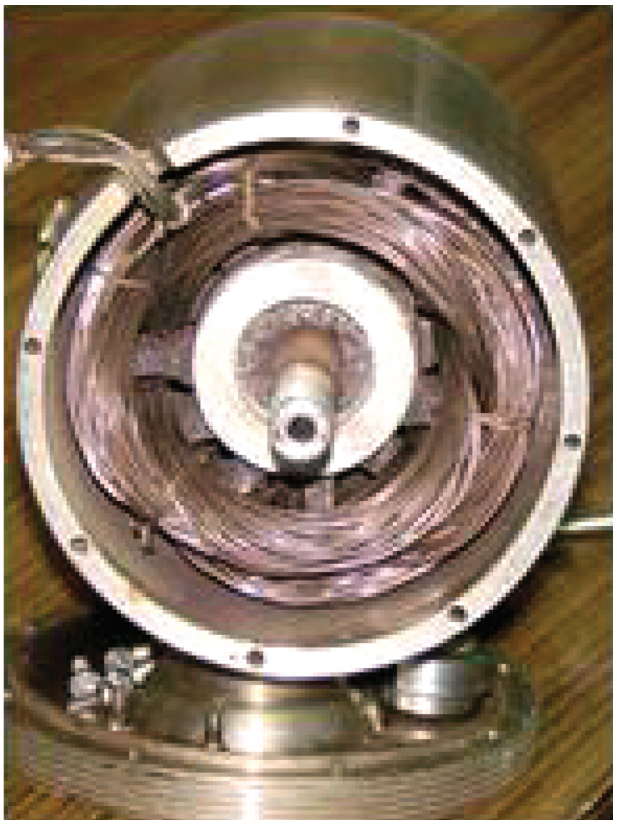

FIG. 12 STATOR OF LOW POWER MOTOR WITH MI CABLE

FIG. 13 MOTOR IN OPEN CONDITION

With reduction in space factor by 50 % because of use of MI cable in stator windings, only 55 turns per phase were possible. Reduction in number of turns led to increase in air gap flux for a rated voltage. High flux resulted in high magnetizing current, leading to higher copper losses and rise in winding temperature. High temperatures in winding did not affect the reliability of motor due to higher thermal withstand capacity of MI cable stator winding. Stator was designed for star

connection and stator flux value was obtained as per following equation.

$$Stator\ voltage\ per\ phase(E_s) = \frac{110}{\sqrt{3}}\ V$$

$$(E_s) = 63.5\ V \quad \text{....(18)}$$

Flux per pole for phase voltage of 63.5 V is

$$\emptyset_m = \frac{E_s}{4.44 \times f \times T_{ph} \times K_w} \quad \text{....(19)}$$

Where

T_{ph} Turns per phase

K_w Winding factor

$$\emptyset_m = \frac{63.5}{4.44 \times 65 \times 55 \times 0.955} \quad \text{....(19)}$$

$$= 0.004189\ Wb$$

Magnetic flux density corresponding to the flux per pole given above is 0.6 T.

3.3 FEM Analysis of High Temperature Induction Motor

FEM analysis of high temperature induction motor was done in FEMM code to check the saturation of various parts of the motor and to predict the rotor torque. Two dimensional model of induction motor with MI cable was simulated using non linear ferromagnetic laminated steel BH curves. Magnetic flux density values in different parts of motors with fixed stator current were simulated and used for predicting torque slip characteristics using Maxwell stress tensor method [7]. Two dimensional model of high temperature induction motor with dimensions given in Section 2 is shown in Figure 14. Constant three-phase currents were applied to the stator windings in model. Stator and rotor core were modeled as silicon steel laminations. The rotor bars were modeled as an aluminum with a conductivity of 34.45 MS/m. Following approximations were made for two dimensional modeling.

- Increase in rotor resistance due to increase in temperature during long operations was neglected.
- Increase in rotor resistance due to end bars was not taken into account.
- Flux leakage off of the rotor ends was not considered.
- Flux leakage off of the stator end turns was not considered.

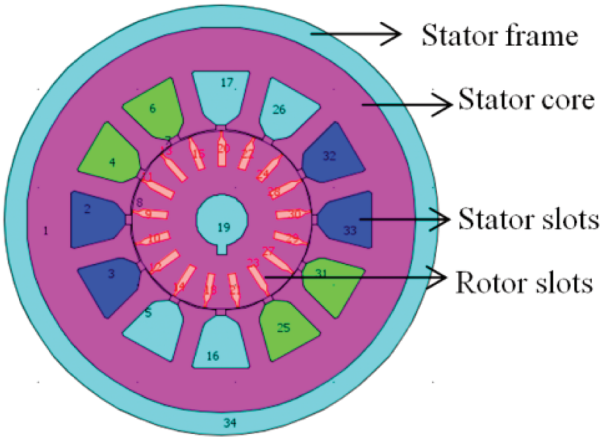

FIG. 14 TWO DIMENSIONAL MODEL OF INDUCTION MOTOR

The analysis was carried out with above mentioned assumptions. Input current density in stator slots and magnetic flux density values in stator and rotor core are shown in Figure 15, Figure 16 & Figure 17 respectively. It can be seen from Figure 17 that magnetic flux density values in rotor core portion between rotor bars and air gap is high but not reaching the saturation point. Electromagnetic torque acting on the rotor is calculated using the Maxwell stress tensor method. Torque verses slip characteristics obtained from FEM analysis for the designed high temperature induction motor is shown in Figure 18.

3.4 Test Results for high temperature induction motor

The induction motor was tested for 2.5 A input current against its rated current of 2 A and the ambient temperature was raised up to 250 ºC. The plot in Figure 19 shows the rise in temperature with respect to time during operation of the

motor. The successful running of motor at 250 ºC proved the design intent. Motor testing was stopped at 250 °C due to temperature limitations of the mechanical bearings used in the motor. The designed motor can be used even for higher temperature operation, if ceramic bearings are used which can withstand higher temperature.

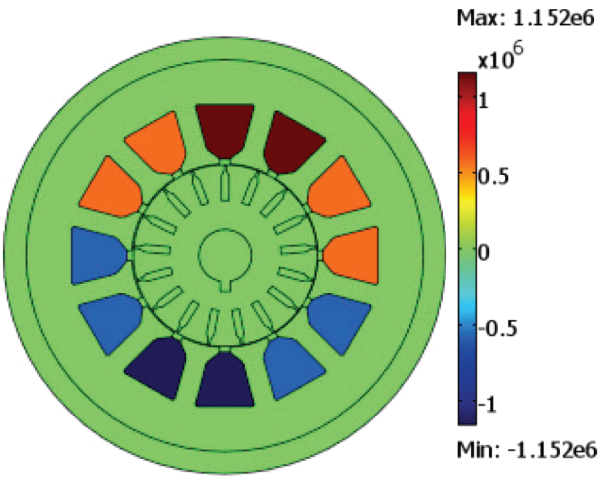

FIG. 15 EXTERNAL CURRENT DENSITY IN STATOR SLOT (A/MM^2)

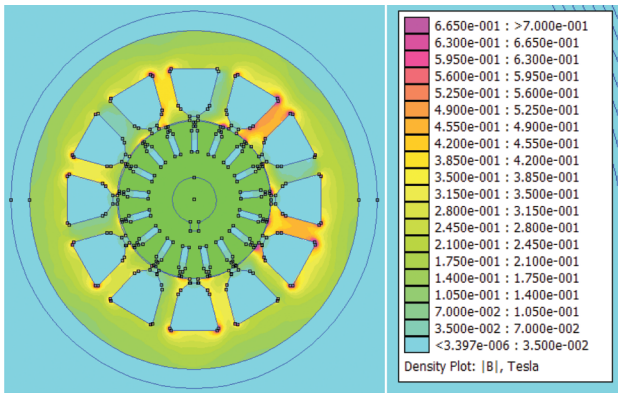

FIG. 16 MAGNETIC FLUX DENSITY PLOT IN STATOR (T)

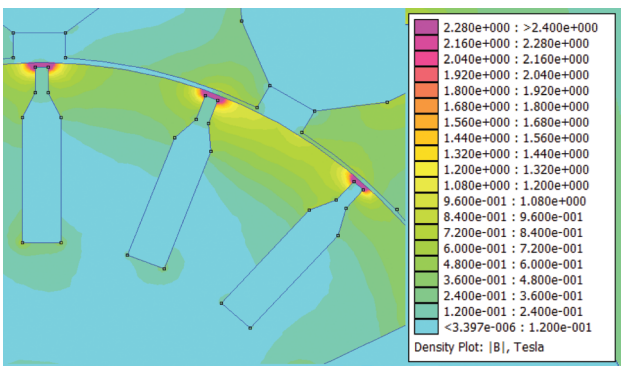

FIG. 17 MAGNETIC FLUX DENSITY PLOT IN ROTOR (T)

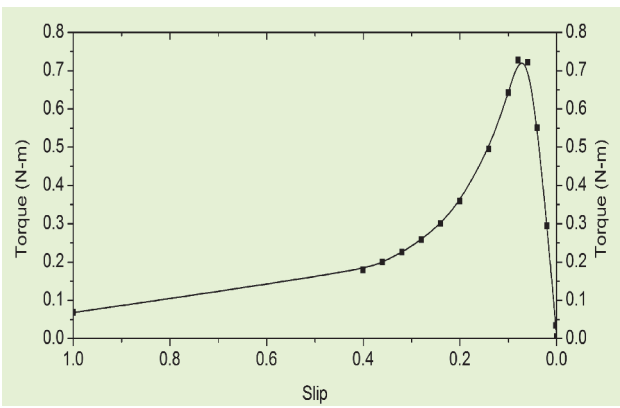

FIG. 18 TORQUE VERSES SLIP CHARACTERISTICS

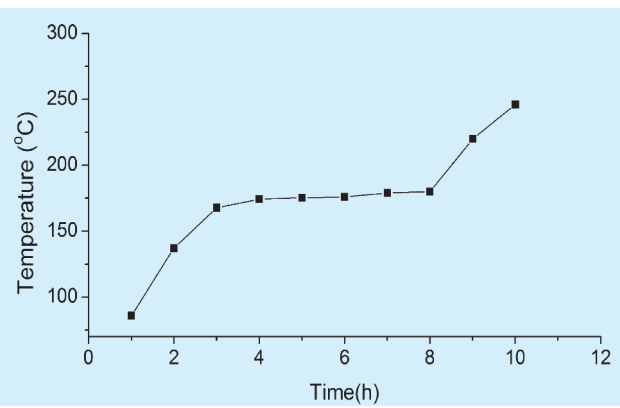

FIG. 19 SURFACE TEMPERATURE VERSES TIME

4.0 CONCLUSIONS

A 50 W three phase induction motor suitable for control systems of PFBR was designed, fabricated and tested. Motor is capable of operating under hostile high temperatures and acidic environment without any external cooling. Motor was tested up to ambient temperature of 250°C with winding temperature withstand capability up to 550 °C. Two dimensional FEM analysis of the tested motor with MI cable as stator windings was carried out. In modeling, torque slip characteristics of the motor, magnetic field distribution in stator and rotor parts of the motor were studied. Design and development of induction motor with MI cable windings for high temperature operation in sodium cooled fast reactor systems was demonstrated successfully. Since mineral insulation is used in the developed motor, it has the potential to operate near the flame also.

REFERENCES

[1] G Srinivasan, K V Suresh Kumar, B Rajendran, P V Ramalingam, The Fast Breeder Test Reactor-Design and operating experiences, Nuclear Engineering and Design, Vol. 236, pp. 796–811, 2006.

[2] S C Chetal, V Balasubramaniyan, P Chellapandi, P Mohanakrishnan, P Puthiyavinayagam, C P Pillai, S Raghupathy, T K Shanmugham, C S Pillai,The design of the prototype fast breeder reactor, Nuclear Engineering and Design, Vol. 236, pp. 852–860, 2006.

[3] J I Sylvia, P V Rao, B Babu, K Madhusoodanan,Development of mutual inductance type sodium level detectors for PFBR, Nuclear Engineering and Design, Vol. 262, pp. 219 – 227, 2013.

[4] V R Babu, R Veerasamy, Sudheer Patri, S Ignatius Sundar Raj, S C S P Kumar Krovvidi, S K Dash, C Meikandamurthy, K K Rajan, P Puthiyavinayagam, P Chellapandi, G Vaidyanathan, S C Chetal, Testing and qualification of Control & Safety Rod and its drive mechanism of Fast Breeder Reactor, Nuclear Engineering and Design, Vol. 240, pp. 1728–1738, 2010.

[5] H Bock, and M Suleiman, Investigations of mineral insulated cables exposed to high temperature and intense gamma radiation, Nuclear Instruments and Methods, North-Holland Publishing Co., Vol. 148, pp. 43-50, 1978.

[6] P Sharma, R Vijayashree, B K Nashine, S K Dash,G Vijayakumar,K A Gopal,S Sosamma, C Babu Rao,K K Rajan,Sensor development for position detection of diverse safety rod of fast reactor, Annals of Nuclear Energy, Vol. 46, pp. 189–196, 2012.

[7] D C Meeker, Finite Element Method, Magnetics, Version 4.2, 11 Apr 2012 Build. http://www.femm.info

[8] J Pedra, I Candela, A Barrera,Saturation model for squirrel-cage induction motors, Electric Power Systems Research, Vol. 79, pp. 1054–1061, 2009.

[9] B Laporte, G Vinsard, J C Mercier, A computation method for induction motors in steady-state, Mathematics and Computers in Simulation, Vol. 38, pp. 369-376,1995.

[10] Y S Chen, Y D Cheng, J J Liao, C C Chiou, Development of a finite element solution module for the analysis of the dynamic behaviour and balancing effects of an induction motor system, Finite Elements in Analysis and Design, Vol. 44, pp. 483 – 492, 2008.

[11] D Sarkar, A K Naskar, Computation of thermal condition in an induction motor during reactor starting, Electrical Power and Energy Systems, Vol. 44, pp. 938–948, 2013.

[12] Y Xie, W Yunyang, 3D temperature field analysis of the induction motors with broken bar fault, Applied Thermal Engineering, Vol. 66, pp. 25-34, 2014.